Cost-Effective Implementation of Multiconformer Transition State Theory for Peroxy Radical Hydrogen Shift Reactions

Møller, Kristian H.

2016

Møller , K H , Otkjaer , R V , Hyttinen , N , Kurten , T C & Kjaergaard , H G 2016 , ' Cost-Effective Implementation of Multiconformer Transition State Theory for Peroxy Radical Hydrogen Shift Reactions ' , Journal of Physical Chemistry A , vol. 120 , no. 51 , pp. 10072-10087 . https://doi.org/10.1021/acs.jpca.6b09370

http://hdl.handle.net/10138/224448
https://doi.org/10.1021/acs.jpca.6b09370

other
publishedVersion

THE JOURNAL OF PHYSICAL CHEMISTRY A

Article

pubs.acs.org/JPCA

Cost-Effective Implementation of Multiconformer Transition State Theory for Peroxy Radical Hydrogen Shift Reactions

Kristian H. Møller,[†] Rasmus V. Otkjær,[†] Noora Hyttinen,[‡] Theo Kurtén,[‡] and Henrik G. Kjaergaard*[,†]

[†]Department of Chemistry, University of Copenhagen, Universitetsparken 5, DK-2100 Copenhagen Ø, Denmark

[‡]Department of Chemistry, University of Helsinki, POB 55, FIN-00014 Helsinki, Finland

Supporting Information

ABSTRACT: Based on a small test system, (*R*)-CH(OH)(OO·)CH_2CHO, we have developed a cost-effective approach to the practical implementation of multiconformer transition state theory for peroxy radical hydrogen shift reactions at atmospherically relevant temperatures. While conformer searching is crucial for accurate reaction rates, an energy cutoff can be used to significantly reduce the computational cost with little loss of accuracy. For the reaction barrier, high-level calculations are needed, but the highest level of electronic structure theory is not necessary for the relative energy between conformers. Improving the approach to both transition state theory and electronic structure theory decreases the calculated reaction rate significantly, so low-level calculations can be used to rule out slow reactions. Further computational time can be saved by approximating the tunneling coefficients for each transition state by only that of the lowest-energy transition state. Finally, we test and validate our approach using higher-level theoretical values for our test system and existing experimental results for additional peroxy radical hydrogen shift reactions in three slightly larger systems.

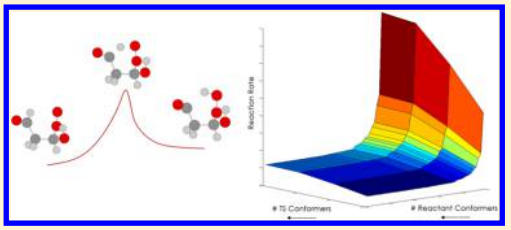

INTRODUCTION

Reduced carbon species are emitted to the atmosphere in enormous quantities from both biogenic and anthropogenic sources.[1−3] These are oxidized in the environment by a diverse set of gas and heterogeneous processes, which greatly reduces their volatility. The low-volatility compounds formed play a key role in the growth of secondary organic aerosol (SOA).[4] While SOA unambiguously affects the Earth's radiative balance via both direct and indirect effects, quantitative assessment of this climate forcing remains a challenge.[5]

Recently it has been shown that autoxidation reactions may play a significant role in the atmospheric oxidation processes leading to the formation and growth of SOA.[6,7] Autoxidation is a series of radical reactions characterized by alternating oxygen addition reactions and intramolecular hydrogen shift reactions. Each O_2 addition leads to a peroxy radical, which in turn abstracts a hydrogen atom from a different location in the same radical species. The initial radical species can be formed following reaction with, e.g., OH or O_3, and the termination step is usually thermal decomposition or a radical−radical reaction.[6]

In the atmosphere, autoxidation competes with reactions with other radicals such as NO, HO_2, and other RO_2 species, and the branching ratios among these pathways depend on the relative reaction rates of the various reactions. For reliable representations of the atmosphere in, e.g., chemistry-transport and ultimately climate models, it is therefore necessary to determine autoxidation reaction rates accurately. For the autoxidation mechanism, the hydrogen shift reactions represent the rate-determining steps, and accordingly, the reaction rates for these types of reactions are central. To assess these reaction rates, quantum-chemical calculations represent an invaluable tool, as they allow treatment of a wide range of systems, conditions, and reactions.

A number of early studies of these hydrogen shift reactions have employed conventional transition state theory, in which the reaction rate is calculated from a transition state and the two conformers connected to it via an intrinsic reaction coordinate (IRC), an approach that we will call IRC-TST.[6,8−12] This approach will almost inevitably overestimate the reaction rate and therefore the relative importance of autoxidation. The reason is that most often the barrier height will be underestimated, as the IRC likely does not connect the lowest-energy conformers. The ability of some conformers to form internal hydrogen bonds can change the reaction barrier by several kcal/mol, which greatly affects the calculated reaction rates.[13] Furthermore, as there are generally more conformers of the reactant than the transition state, the overall transition state partition function is usually smaller than the overall reactant partition function, which decreases the rate.

Within the framework of TST, the presence of multiple conformers can be taken into account by multiconformer transition state theory (MC-TST).[14] The MC-TST reaction rate constant can be considered a sum of the individual IRC-TST reaction rate constants, each weighted by the Boltzmann population of the corresponding reactant conformer. We show (see section S1) that this description is equivalent to the form in which MC-TST is usually presented. Recently, MC-TST has

Received: September 16, 2016
Revised: November 29, 2016
Published: November 30, 2016

DOI: 10.1021/acs.jpca.6b09370
J. Phys. Chem. A 2016, 120, 10072−10087

started to emerge as a method in the study of atmospheric autoxidation.[15−19]

For most systems, computational limitations necessitate approximations to the full MC-TST treatment. We have therefore developed a guideline for the practical implementation of MC-TST for the atmospherically important unimolecular hydrogen shift reactions in peroxy radicals. The goal is to minimize both the computational and human time required for these types of calculations while maintaining high accuracy. The approach is intended for hydrogen shift reactions of small to medium-sized peroxy radicals (around 5−15 non-hydrogen atoms) at atmospherically relevant temperatures. The challenge upon progressing to larger systems is twofold: First, larger, more flexible molecules have more conformers that need to be considered. For example, in a recent study of O_3-initiated cyclohexene autoxidation, the total number of conformers initially generated was on the order of 100 000.[17] Second, the scaling of the quantum computational methods means that the computational cost of each conformer increases significantly. For instance, the computational effort of the CCSD(T) energy calculation scales approximately as the seventh power of the system size.[20] While higher-level treatment may be possible for the initial reactions of many species of atmospheric relevance, during autoxidation the size of the species studied continuously increases by sequential addition of molecular oxygen, and having a systematic approach that can consistently treat all reactions along the way is very desirable.[17] Apart from atmospheric science, the importance of hydrogen shift reactions has also been acknowledged in combustion chemistry, and we will therefore also assess our approach at elevated temperatures.[21−24]

We have carried out a systematic investigation on a small test system for which a high-level treatment is possible. We have chosen the 1,5-aldehydic hydrogen shift in (*R*)-1-hydroxy-3-oxopropyl-1-peroxy radical, (*R*)-CH(OH)(OO·)CH_2CHO, shown schematically in Figure 1. While the radical is small enough for a high-level treatment including coupled-cluster optimization, it remains representative of peroxy radicals of atmospheric interest. For instance, it closely resembles a radical formed in the OH-initiated oxidation of acrolein. The motif of a peroxy group radical abstracting an aldehydic hydrogen is usually fast, as observed in, e.g., methacrolein.[11,25] Furthermore, it has the ability to form internal hydrogen bonds, which can be important for the conformational sampling.[13]

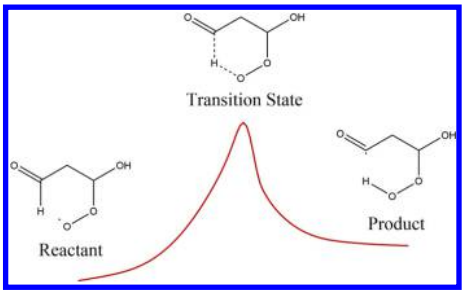

Figure 1. Overview of the 1,5-aldehydic hydrogen shift reaction in (*R*)-1-hydroxy-3-oxopropyl-1-peroxy radical. The forward and reverse barriers are 19 and 14 kcal/mol, respectively, for the lowest-energy conformers at the ωB97X-D/aug-cc-pVTZ level of theory.

As an additional reaction, we have studied the reverse 1,5-hydrogen shift to re-form the peroxy radical, as the relative rate between the forward and reverse reactions is important for the product distribution for systems with multiple, competing reactions. Despite having studied both the forward and reverse reactions, we use the convention of referring to the peroxy radical as the reactant and the acyl radical as the product, corresponding to the reaction from left to right in Figure 1. For these two reactions, we have tested the effect of a wide range of parameters, including the method used in the initial conformer search, the use of various cutoffs along the progression toward higher-level calculations, and the method used for calculating the energy barrier.

On the basis of our observations, we have developed a guideline for the implementation of MC-TST for hydrogen shift reactions of peroxy radicals. This guideline is applied to three additional peroxy radical hydrogen shift reactions for which experimental results are available.

THEORY AND METHODS

Systematic conformer searches were carried out using Spartan'14 and the molecular mechanics (MMFF and SYBYL) and semiempirical (AM1, MNDO, PM3, PM6, and RM1) methods available in this program as well as density functional theory (DFT) at the B3LYP/6-31+G(d) level.[26−40] These were selected to cover a wide range of different methods and because of their availability in Spartan. While B3LYP is known to lack a proper description of dispersion interactions, it was chosen because its implementation is usually very efficient and it has been widely tested.[41−43] Furthermore, it has been found to accurately predict the energy ordering of conformers.[17,44,45]

In a systematic conformer search, every nonterminal bond is rotated a certain number of times, and an optimization is conducted to see if the resulting structure represents a minimum on the potential energy surface. The default number of rotations in Spartan is 3 for bonds between sp^3 hybridized atoms and 2 for bonds between sp^2 hybridized atoms. For the transition states, constraints were placed on selected bond lengths before the conformer search was initiated, as no conformer sampling algorithms or molecular mechanics force fields for transition state structures were available. While transition state force fields (TSFFs) do exist, they need to be parametrized specifically for the reaction studied.[46,47] In the constrained conformer searches, tests showed that constraining only the bonds being formed and broken is not enough and that at least one more constraint is needed for effective conformer sampling of the transition state (see Table S5). Molecular mechanics is sensitive to the bonds drawn in the input, and for the transition state searches, the bonding pattern of the reactant was retained but with the bond lengths of the transition state.

All of the conformer searches were carried out using the keywords "searchmethod = systematic" to ensure systematic conformer searches and "keepall" to prevent removal of conformers. For the semiempirical methods, the keywords "scfcycles = 500" and "geometrycycles = 500" were employed to increase the number of cycles for the SCF and geometry convergence, as the default number of cycles was not enough for all conformers.

By default, MMFF as implemented in Spartan'14 treats RO_2 oxygen radicals as anions, which greatly affects the conformer sampling. Generally, the treatment of radicals by MMFF and most other standard force fields is inadequate, as they have not been parametrized for these.[27,33,48−50] Therefore, further calculations were carried out by tweaking the treatment of

DOI: 10.1021/acs.jpca.6b09370
J. Phys. Chem. A 2016, 120, 10072−10087

the radical centers using two different keywords: The keyword "ffhint = X~~+0" specifies the charge of atom X to be 0, as is correct for the radical species treated here. Similarly, the keyword "ffhint = X~~y" changes the molecular mechanics atom type of atom X to type y. In our calculations, X is the radical center, and several different atom types, y, of this were tested. These two approaches will be denoted as MMFF-charge and MMFF-type, respectively. They are described in the "Mechanics FAQs" section of Spartan'14.

The molecular mechanics and semiempirical conformer searches were followed by DFT optimizations carried out using Gaussian 09, revision D.01.[51] Subsequent frequency calculations were carried out to confirm the character of the stationary points identified (no imaginary frequencies for reactants and products and one imaginary frequency for transition states).

The DFT calculations were carried out using two functional/basis set combinations: B3LYP/6-31+G(d) and ωB97X-D/aug-cc-pVTZ.[39,40,52−57] With the aug-cc-pVTZ basis set (abbreviated aVTZ), the calculations were carried out with the keywords "opt = verytight" and "int = ultrafine". The two levels of theory were chosen because they have previously shown good agreement with much higher level calculations for relative energies between conformers (B3LYP) and reaction barriers (ωB97X-D), respectively.[12,17,44,45,52]

For the transition states, the additional optimization keywords "calcfc" and "noeigentest" were used to guide the optimization by calculating the force constants in the first optimization step and suppressing termination of the calculation even if more than one imaginary frequency was calculated initially. For the transition states, the B3LYP/6-31+G(d) TS optimization was preceded by a constrained optimization with the same constraints as employed in the conformer search. Bypassing the constrained optimization was tested but found to be very ineffective (see Table S7).

The "opt = calcall" and "scf = qc" keywords were employed in a limited number of cases for which convergence was an issue or imaginary frequencies were observed for the reactant or product. All of the thermodynamic calculations were carried out at 298.15 K and 1 atm, unless otherwise stated.

Molpro 2012.1 was used for single-point energy calculations on top of the ωB97X-D/aVTZ-optimized structures at the ROHF-ROCCSD(T)-F12a/cc-pVDZ-F12 level (abbreviated F12) for more accurate energies.[58−63] ROCCSD(T)-F12a has shown very good agreement with higher-level results with much faster basis set convergence.[61] In accordance with recommendations, the calculations were carried out using "gem_beta = 0.9", which sets the value of the geminal Slater exponent β in the F12 correlation factor to 0.9.[63] To test the quality of the ωB97X-D/aVTZ geometry, the lowest-energy conformers of the reactant, transition state, and product were optimized at the F12 level to assess the error introduced by doing only single-point F12 calculations.

Transition State Theory. Chemical reaction rate constants were calculated using transition state theory including quantum-mechanical tunneling. In transition state theory, the reaction rate constant, k, for a unimolecular reaction is given by[8]

$$k = \kappa \frac{k_B T}{h} \frac{Q_{TS}}{Q_R} \exp\left(-\frac{E_{TS} - E_R}{k_B T}\right) \quad (1)$$

where κ is the quantum-mechanical tunneling coefficient, k_B is Boltzmann's constant, T is the absolute temperature, h is Planck's constant, Q_{TS} and Q_R are the partition functions of the transition state and reactant, respectively, and E_{TS} and E_R are the corresponding zero-point-corrected electronic energies of the transition state and reactant. The difference in energy between the reactant and transition state is the reaction barrier.

For all but the smallest or most rigid systems, a number of conformers of the reactant, TS, and product exist (see Figure 2), which can be taken into account in different ways. In the method we will refer to as intrinsic reaction coordinate TST (IRC-TST), one conformer of the transition state is used along with the conformers of the reactant and product connected to it via an IRC. As we carried out the conformer sampling, we used the lowest-energy conformer of the transition state in the IRC-TST calculations. A better approximation than IRC-TST is to calculate the reaction rate constant from the lowest-energy conformers of the reactant, transition state, and product, an approach that we call lowest-conformer TST (LC-TST).

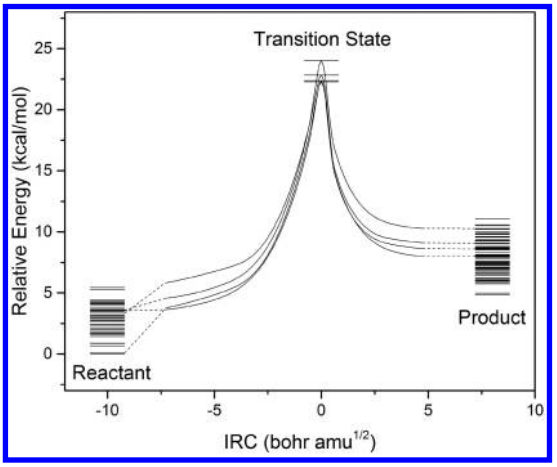

Figure 2. Overview of the energetics of the system studied here showing the individual conformers of the reactant, transition state, and product as well as the IRCs. The dashed lines connect the IRCs to the corresponding stationary points. All values were calculated at the ωB97X-D/aVTZ level.

Multiconformer transition state theory (MC-TST) can be used to include the effect of multiple conformers within the framework of TST.[14] In a multiconformer system, not all reactants will be in a conformation with a path across the reaction barrier, as shown in Figure 2. The MC-TST reaction rate can therefore be calculated as a sum of IRC-TST reaction rate constants, one for each transition state, weighted by the Boltzmann populations of the corresponding reactants:

$$k = \sum_{i}^{\text{all TS conf.}} F_i \times k_{\text{IRC}_i} \quad (2)$$

where the sum runs over all transition states, k_{IRC_i} is the IRC-TST reaction rate constant (including tunneling) of conformer i (calculated as in eq 1), and F_i is the relative Boltzmann population of the reactant connected to TS_i via the IRC. The equation assumes that the barriers for interconversion between the various conformers are low enough to allow these to be in internal equilibrium. For ease of calculation, the MC-TST expression in eq 2 can be rewritten (see section S1) in the following more convenient form:

DOI: 10.1021/acs.jpca.6b09370
J. Phys. Chem. A 2016, 120, 10072−10087

$$k = \frac{k_B T}{h} \frac{\sum_i^{\text{all TS conf.}} \kappa_i \exp\left(-\frac{\Delta E_i}{k_B T}\right) Q_{TS,i}}{\sum_j^{\text{all R conf.}} \exp\left(-\frac{\Delta E_j}{k_B T}\right) Q_{R,j}} \exp\left(-\frac{E_{TS,0} - E_{R,0}}{k_B T}\right) \quad (3)$$

In eq 3, the summations in the numerator and denominator are carried out over all conformers of the transition state and reactant, respectively. κ_i is the tunneling coefficient calculated from the path connected to TS_i. ΔE_i represents the zero-point-corrected energy of transition state conformer i relative to the lowest-energy transition state conformer, and $Q_{TS,i}$ is the total partition function of transition state conformer i. ΔE_j and $Q_{R,j}$ are the corresponding values for reactant conformer j. $E_{TS,0}$ and $E_{R,0}$ in the final factor refer to the zero-point-corrected energies of the lowest-energy conformers of the transition state and reactant, respectively. In the case of only one reactant and transition state, eq 3 reduces to the well-known TST expression in eq 1. The assumption that tunneling is the same for all reaction paths leads to the form in which MC-TST is usually presented:[8,14]

$$k = \kappa \frac{k_B T}{h} \frac{\sum_i^{\text{all TS conf.}} \exp\left(-\frac{\Delta E_i}{k_B T}\right) Q_{TS,i}}{\sum_j^{\text{all R conf.}} \exp\left(-\frac{\Delta E_j}{k_B T}\right) Q_{R,j}} \exp\left(-\frac{E_{TS,0} - E_{R,0}}{k_B T}\right) \quad (4)$$

The energies and partition functions in the MC-TST expression can be calculated at different levels of electronic structure theory. Table 1 provides an overview of the various levels of electronic structure theory employed for calculation of the TST reaction rate constants in this work. Unless otherwise stated, the reaction rate constants presented in this work do not include tunneling, as this was treated separately.

Table 1. Overview of the Levels of Electronic Structure Theory Employed in the Calculation of Reaction Rate Constants along with the Names Used To Refer to Them

Name	Description
B3LYP	B3LYP/6-31+G(d) partition functions and zero-point-corrected energies for all conformers included.
ωB97X-D	ωB97X-D/aVTZ partition functions and zero-point-corrected energies for all conformers included.
F12-lowest	ROHF-ROCCSD(T)-F12a/cc-pVDZ-F12//ωB97X-D/aVTZ single-point energies plus ωB97X-D/aVTZ ZPVE for the reaction barrier[a] and ωB97X-D/aVTZ zero-point-corrected energies for the relative energies between conformers[b] and for partition functions.
F12-all	Like F12-lowest but with F12 single-point energies combined with ωB97X-D/aVTZ zero-point corrections for all conformers.

[a]The energy difference between the lowest-energy conformers of the reactant and TS. [b]In the sum of partition functions.

Tunneling. Because of the low mass of the hydrogen atom being transferred, quantum-mechanical tunneling is important for most hydrogen shift reactions.[64] Because MC-TST is a Boltzmann-weighted sum of IRC-TST reaction rates, the correct way to include tunneling is to use the corresponding tunneling coefficient for each of these, as shown in eq 3. However, this requires calculation of a tunneling coefficient for each of the pathways across the barrier, which can be computationally expensive. Optimally, for simplicity and to save computational time, we want, as an approximation, to use only one tunneling coefficient, as shown in eq 4.

As shown in eq 3, each of the tunneling coefficients is weighted by the Boltzmann weight of the corresponding transition state multiplied by its partition function. Under the assumption that the partition functions of different conformers are similar, this means that the most important tunneling factor is the one related to the lowest-energy transition state, and the most logical approximation is to use only this. For this approximation to be good, either the tunneling coefficients calculated from the different transition states must be similar or the Boltzmann population of the lowest-energy transition state must be significantly higher than that of the other transition states.

Assessment of various methods for calculating tunneling coefficients and the calculation of highly accurate tunneling coefficients are not the focus of this paper, but tunneling is included to provide reasonable reaction rates. For the actual tunneling coefficient, we have used the widely employed 1D Eckart tunneling approach.[65] Eckart tunneling is a simple one-dimensional tunneling approach in which the tunneling coefficient is calculated by solving the Schrödinger equation for an asymmetrical one-dimensional Eckart potential.[65] It is the exact solution to an approximate potential derived from the barrier heights on both sides of the transition state and its imaginary frequency. Eckart tunneling has previously been shown to yield results in good agreement with multidimensional small-curvature tunneling for hydrogen shift reactions.[66,67]

The imaginary frequency of the transition state was calculated using ωB97X-D/aVTZ, while the barriers were calculated from F12 single-point electronic energies with ωB97X-D/aVTZ zero-point vibrational corrections. With these, MATLAB R2013a was used to calculate the Eckart tunneling coefficients.[68] We will refer to the level of electronic structure theory for the Eckart calculations as F12/ωB97X-D. As a test, the IRC used to identify the conformers connected to the transition state were calculated using the "calcall" keyword at both the B3LYP/6-31+G(d) and ωB97X-D/aVTZ levels of theory. Higher-level multidimensional tunneling approaches were not assessed. While accurate tunneling coefficients are important for absolute rates, higher-level tunneling coefficients would not affect the conclusions drawn in this work.

Hindered Rotations. By default, Gaussian 09 treats all vibrations as harmonic oscillators, so unless otherwise stated, all of the reaction rate constants in this work were calculated using harmonic oscillator partition functions. However, low-frequency vibrations such as internal torsions are not well described by that model, and therefore, several other approaches for calculating the partition functions were assessed. The "Freq = HinderedRotor" keyword in Gaussian 09 automatically identifies internal rotations and calculates the corrections to the partition functions and thermodynamic properties based on three different approximations for uncoupled (1D) hindered rotors: Pitzer and Gwinn, Truhlar, and McClurg.[69−73] All three approaches interpolate between the quantum harmonic oscillator in the low-temperature limit and the free internal rotor in the high-temperature limit and differ only in the interpolation function (see section S2).[69] To avoid double-counting, the calculated hindered rotor corrections to the partition functions were divided by the "Multi-

DOI: 10.1021/acs.jpca.6b09370
J. Phys. Chem. A 2016, 120, 10072−10087

plicity", which accounts for the effect of access to other potential energy wells. These other minima represent different conformers and are therefore already being taken into account.

Multistructural hindered rotor calculations based on coupled anharmonic torsional potentials (MS-T) were carried out using MSTor as described in the MSTor manual.[74−77] As for the 1D hindered rotor approaches, the MS-T approach employs a combination of quantum and classical contributions to the partition function.[76]

A full quantum-mechanical treatment of the vibrational partition function requires simultaneous scans over all of the torsional angles to obtain the full coupled torsional potential energy surface. As the number of energy evaluations required for this grows exponentially with the number of torsional degrees of freedom, it is not a viable option. However, it has been found that simpler approximations such as the ones included here can perform reasonably well.[78,79] In the MC-TST expression for the rate constant (eq 4), the partition functions of the transition state are divided by the partition functions of the reactant. The uncertainties in the calculated partition functions are therefore expected to at least partially cancel.

Identifying Unique Conformers. To distinguish between conformers at a given level of theory, we have written a bash-wrapped Python script (given in section S3) comparing the energy (electronic or zero-point-corrected), ΔE, dipole moment, $\Delta\mu$, and root-mean-square-deviation of atomic positions following a Kabsch rotation, RMSD(geo).[80] The last of these was implemented directly from Github.[81] In its current form, the RMSD script fails to mark conformers as identical if the atom labels are no longer identical after, e.g., methyl torsion, but for the system studied here that does not cause problems. Similarly, it marks mirror images of the same conformer as different, which again is not a problem for this system.

Conformers were identified as duplicates when they were below a certain threshold for all three criteria. The optimal threshold depends on the system and the convergence criteria for the electronic structure calculation. Too-tight criteria would mark too many conformers as unique and thereby lead to double counting of conformers, while too-loose criteria would result in loss of conformers. By employing three different criteria to distinguish the conformers, one can loosen the threshold of each of the three criteria while decreasing the risk of losing conformers.

Plots of the geometrical RMSD as well as energy and dipole moment differences between pairs of conformers (Figures S1 and S2) show a clear separation between duplicate structures and different conformers. On the basis of these plots, cutoff values of $\Delta E = 1 \times 10^{-5}$ hartree, $\Delta\mu = 1.5 \times 10^{-2}$ D, and RMSD(geo) $= 2 \times 10^{-2}$ Å were chosen as criteria for identifying duplicates (see section S4). The uniqueness of the structures obtained was confirmed by visual inspection. While we expect these cutoffs to be suitable for systems similar to the one studied here, plots similar to the ones in section S4 can be used to check the validity and potentially find cutoffs that are more suitable for the system studied. Even for systems for which the geometrical comparison is not applicable for the reasons outlined above, we found that suitable cutoffs on energy and dipole moment are enough to effectively identify pairs of duplicate structures.

RESULTS AND DISCUSSION

The following sections assess the effect of a wide range of parameters on the calculated reaction rate constant: conformer searching, approaches to electronic structure and transition state theory, and a cutoff in the number of conformers included in the MC-TST calculation. All of these considerations lead us to propose guidelines for the implementation of MC-TST. For the test system, the approach is assessed by comparison to a high-level theoretical benchmark, which includes F12 optimizations. In addition, our approach is applied to three additional peroxy radical hydrogen shifts in slightly larger systems for which experimental results are available.

Conformer Searching of the Reactant and Product. In Figure 3, we compare the number of conformers obtained from the various molecular mechanics and semiempirical conformer searching methods available in Spartan'14. For comparability, the conformer searches are followed by B3LYP/6-31+G(d) optimizations of all structures. The results are given as a fraction relative to the combined total of all conformers obtained with all methods. Combining all of the various conformer searching methods, we have identified 48 unique conformers of the reactant and 81 unique conformers of the product at the B3LYP/6-31+G(d) level of theory. The figure also includes the result obtained by bypassing the low-level conformer search and doing a B3LYP/6-31+G(d) optimization directly on the systematically generated structures. However, this procedure requires DFT optimizations of a very large number of structures and is viable only for very small systems. For MMFF, the results obtained when enforcing the correct (neutral) charge on the radical center, MMFF-charge, and the results obtained with the best radical atom type of the ones tested, MMFF-type, are included in the figure. For all methods, the default value of threefold rotation around each of the nonterminal bonds was employed for this comparison. All conformer searches for the reactant and product, respectively, were started from the same geometry, which had been drawn by hand in the graphical user interface of Spartan.

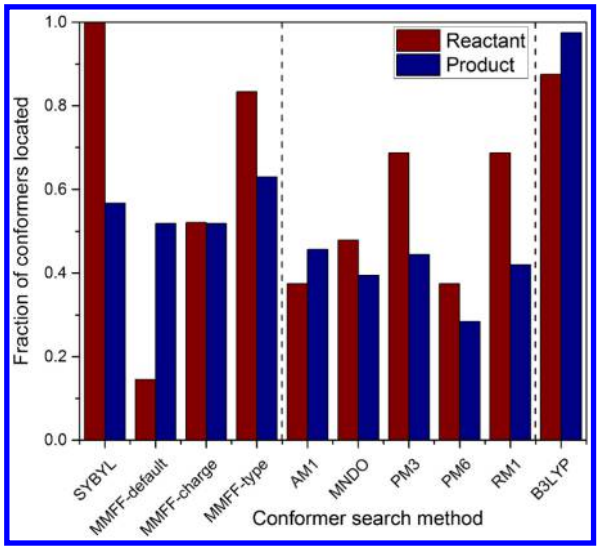

Figure 3. Fractions of conformers of the reactant and product located with various search methods calculated relative to all conformers. "All conformers" is defined here as the sum of unique conformers located with all search methods combined. The dashed vertical lines divide the molecular mechanics methods on the left, the semiempirical methods in the center and the DFT method (B3LYP/6-31+G(d)) on the right.

As can be seen in in Figure 3, none of the conformer searching methods locate all of the conformers of both the

DOI: 10.1021/acs.jpca.6b09370
J. Phys. Chem. A 2016, 120, 10072−10087

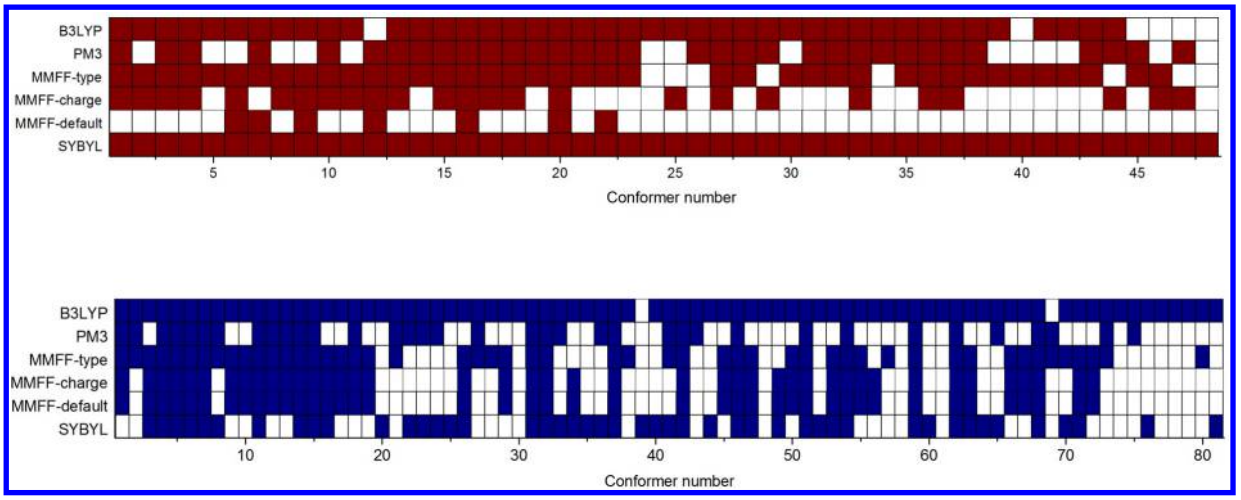

Figure 4. Conformers of the reactant (top panel, red) and product (bottom panel, blue) located (filled) and missed (empty) using selected conformer searching methods. Conformers are ordered relative to B3LYP/6-31+G(d) zero-point-corrected energies with the lowest energy at the left.

reactant and product. The only method that does consistently well for both the reactant and product is B3LYP. However, even B3LYP does not locate all of the conformers, and more importantly, for larger systems it is not computationally viable.

It is clear that the molecular mechanics and semiempirical methods all have significant problems locating the conformers of the open-shell systems studied. Until cheap methods that are better suited for treating open-shell systems become more widely implemented, we have to accept some loss of conformers and can only attempt to minimize this and assess the error introduced by the incomplete conformer sampling. Generally, no better performance is observed for the semiempirical methods compared with the molecular mechanics methods. For the semiempirical methods, PM3 appears to do best, while PM6 appears to perform the worst.

Because of the Boltzmann weighting in the MC-TST expression, the importance of a conformer decreases with increasing energy. Figure 4 provides a detailed overview of the performance of selected conformer searching methods in terms of which specific conformers they succeed and fail to locate. The conformers are sorted by increasing energy to the right, which means that conformers to the left have the highest Boltzmann weights and influence the reaction rate the most. A full overview of the energies of all the different conformers and the details of which methods locate which conformers can be seen in section S5.1.

In both Figures 3 and 4, the worst overall performance is observed for MMFF with default parameters for the reactant, as it locates less than 20% of the conformers and misses the five lowest-energy conformers. As mentioned earlier, the problem is that MMFF treats the oxygen radical as an anion, which strongly affects the conformer sampling.

However, as is clear from the figures, changing the charge (MMFF-charge) or atomic type (MMFF-type) improves the results for MMFF significantly. For the peroxy radical, correcting the charge more than triples the number of conformers located. For the acyl radical, no difference is observed, as the default parameters already include the correct charge and MMFF-default performs quite well. For other carbon-centered radicals, however, changing the charge can be important. Even better results are obtained by changing the atom type assigned to the radical atom, the approach denoted MMFF-type. With the MMFF force field, Spartan erroneously assigns peroxy radical oxygens the MMFF atomic type "32", which corresponds to a carboxylate oxygen. The default type for the acyl radical is type " 203", which is a Spartan extension to the original MMFF force field. For the peroxy radical oxygen we have tested types 6 ("generic divalent O") and 7 ("generic C═O") and for the acyl radical types 1 ("alkyl carbon sp^3"), 2 ("generic sp^2 C"), 3 ("generic carbonyl carbon"), and 4 ("allenic carbon"). The best results were obtained for types 6 and 3 for the reactant and product, respectively, which correspond to the types that would be expected without the radical center present, i.e., with a hydrogen bonded to the atom instead. These are the types included in Figure 3. For more detailed results from the testing of atom types, see section S5.2.

In Figures 3 and 4, we show that not only does MMFF-type locate a large fraction of conformers of both the reactant and product, it locates most of the important low-energy conformers. The method locates the 23 and 19 lowest-energy conformers of the reactant and product, respectively. The good performance is in part due to the fact that of the different atom types tested, only the best is included in the comparison in the figure. While such a search for the optimal atom type during a routine calculation is not viable, this suggests that with an extensive study of the optimal atom types for various radical species, MMFF-type would be a very good choice for conformer searching of radical species.

The data in Figure 3 suggest that besides B3LYP, SYBYL has the best overall performance, with the highest fraction of conformers captured for the peroxy radical (100%) and third highest for the acyl radical (56%). However, from Figure 4 it is clear that for the acyl radical SYBYL misses the two lowest-energy (and therefore most important) conformers plus another four of the 15 lowest-energy conformers.

For this system, test calculations suggest that increasing the number of rotations in the systematic conformer search beyond the default of 3 for all nonterminal bonds has very little effect on the number of conformers located, as shown in section S5.3. Similarly, starting the conformer search of the reactant or product from a geometry optimized with B3LYP/6-31+G(d) rather than a structure simply drawn by hand seems to change very little (see section S5.4).

DOI: 10.1021/acs.jpca.6b09370
J. Phys. Chem. A 2016, 120, 10072−10087

For the DFT optimization directly following the conformer search, no systematic difference is observed between using B3LYP and ωB97X-D (both with the 6-31+G(d) basis set) in terms of the number of conformers located. However, as B3LYP is a simpler functional, the optimizations are significantly faster (see section S5.5).[52]

Conformer Searching of the Transition State. A slightly different approach is needed for the conformer search of the transition states, as we do not have access to any conformer searching methods that can treat these directly. To capture the structure of the transition states, conformer searches were carried out after constraining several bond lengths in a transition state structure. However, all of the semiempirical methods available in Spartan'14 failed to converge for the constrained optimizations, and therefore, no results were obtained for these. None of the molecular mechanics methods had problems with convergence.

For this small system, the total number of transition states is limited to four, and they are shown in Figure 5. Constraining

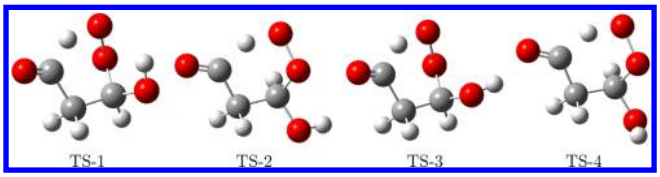

Figure 5. ωB97X-D/aug-cc-pVTZ-optimized structures of the four unique transition states sorted by zero-point-corrected energy at the same level, with the lowest-energy structure at the left.

only the C···H and H···O bonds in the C···H···O−O−C transition state moiety does not appear to be enough, as this approach locates only one of the four transition states with the various molecular mechanics methods, corresponding to the one being input. However, searches with both three (C···H, H···O, and O−O) and four (C···H, H···O, O−O, and O−C) constraints located all four transition states for all four molecular mechanics methods: SYBYL, MMFF-default, MMFF-charge, and MMFF-type. A comparison of the bond lengths for the reactant, transition state, and product shows that besides the bonds being formed and broken in the reaction (the C···H and H···O bonds), the O−O bond length is the one that changes the most among the reactant, transition state, and product (see section S5.7). Therefore, we suggest constraining those three bonds in conformer searching of transition state structures of hydrogen shift reactions of peroxy radicals. The challenge of using constrained conformer searches for the transition state is that a large number of the conformers located in the conformer search revert to the same structure after a B3LYP/6-31+G(d) optimization, which wastes significant amounts of computational time. However, no better method has yet been found, and improvements may require the development of transition state force fields parametrized specifically for peroxy radical hydrogen shift reactions.

For the B3LYP optimizations of the transition states, we find that it is very advantageous to follow the conformer search by a constrained optimization toward a minimum with the same constraints as in the conformer search. Preceding the transition state optimization with an optimization using the much more efficient minimization algorithm both reduces the total CPU time for the optimizations significantly (around a factor of 4 in this case) and leads to fewer structures ending up as transition states of other reactions (see section S5.8). Furthermore, this allows elimination of duplicate conformers earlier, which further reduces the CPU time.

Starting the conformer search from a B3LYP-optimized transition state structure rather than a transition state constructed by the "Guess Transition State" function in Spartan'14 similarly represents a sensible choice, as the structures resulting from the conformer search are closer to the ones subsequently optimized and the constrained optimizations therefore require fewer restarts (see section S5.9). This is not surprising, as the constrained bond lengths are in better agreement with the B3LYP-optimized structures and represent better guesses of the transition state structure. For systems with multiple hydrogen atoms on the carbon atom from which the abstraction occurs, it is important to consider whether different conformers can be obtained by abstracting the different hydrogens.

Effect of Conformer Search on Reaction Rate Constants. In Figure 6, we compare the MC-TST reaction

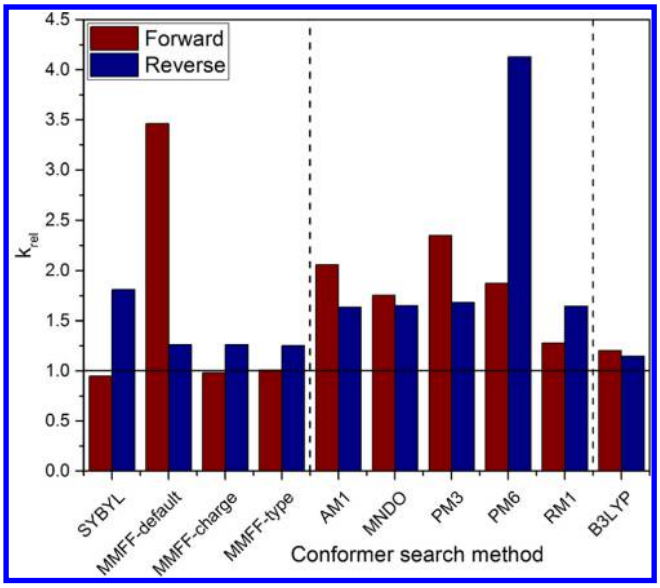

Figure 6. Relative B3LYP MC-TST reaction rate constants, k_{rel}, with the reactant (forward) or product (reverse) conformers found by the different search methods relative to the rate constant obtained using all conformers. All four transition states were used in all of the calculations. The dashed vertical lines divide the molecular mechanics methods on the left, the semiempirical methods in the center, and the DFT method (B3LYP/6-31+G(d)) on the right. All of the reaction rates were calculated following B3LYP/6-31+G(d) optimizations and frequency calculations of all structures.

rate constants obtained with the reactant and product conformers located by a given conformer searching method to the rate that is obtained by including all of the conformers. The rates were calculated at the B3LYP/6-31+G(d) level of theory. All four transition states were included in all of the calculations. This means that only the conformer searching of the reactant and product is being probed, and missing conformers will lead to overestimation of the reaction rate. For clarity, the reaction rate constants have been divided by the reaction rate constants obtained when using all conformers. The value below 1 obtained for, e.g., SYBYL is due to small unsystematic variations in the low-frequency vibrations, to which the rate is quite sensitive. Despite the relatively large variation in the performance of the various conformer search

DOI: 10.1021/acs.jpca.6b09370
J. Phys. Chem. A 2016, 120, 10072−10087

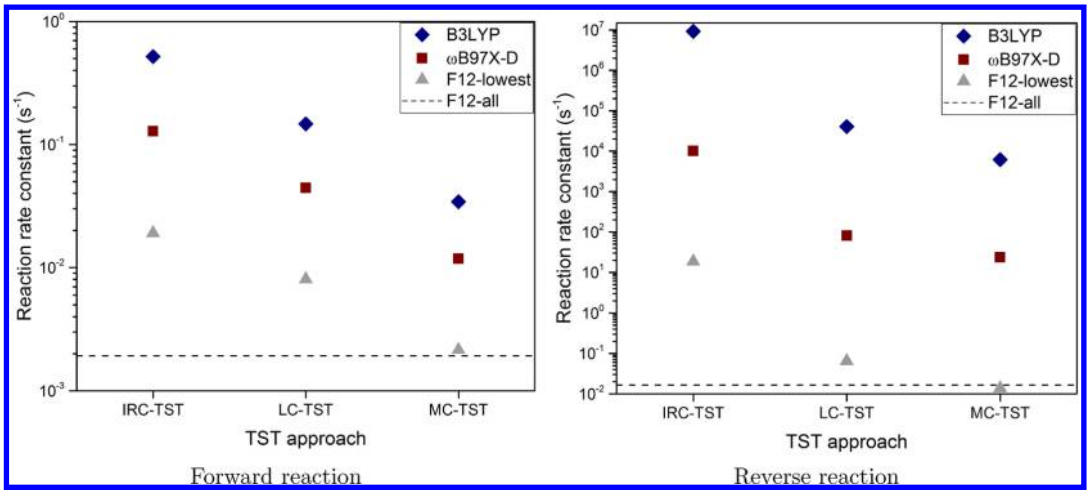

Figure 7. Forward (left) and reverse (right) reaction rate constants (in s^{-1}) calculated using different combinations of electronic structure theory and TST. The dashed horizontal line corresponds to the benchmark of MC-TST F12-all. The MC-TST results include all conformers located in total.

methods, nearly all of the reaction rate constants are within a factor of 2 of the rate constant obtained with all conformers.

The figure again highlights the unimpressive performance of the semiempirical methods relative to the much cheaper molecular mechanics methods. Two results stand out as being far worse than the others: The forward rate with MMFF-default and the reverse rate with PM6. Both deviations are caused by the method missing a large number of the important low-energy conformers. On the other hand, MMFF-charge, MMFF-type, and B3LYP provide very good results for both the forward and reverse reactions.

Missing a few conformers seems inevitable and generally introduces only little error relative to the optimal, but practically impossible, goal of locating all of the conformers. With an extensive study of the optimal atom types for various radical species, MMFF-type appears to be a good choice for conformer searching of radical species. Until such a study is carried out, however, we propose the use of MMFF with the correct charge enforced (MMFF-charge) for conformer searches, as this is an easy, general, and very effective fix. Alternatively, SYBYL appears to be a very reasonable alternative. In principle, one could combine the results from multiple conformer searching methods, but this may not be computationally feasible. The force fields tested here, however, are not parametrized for radicals, and force fields better suited for those may be necessary to reduce the risk of missing important conformers.

Effect of TST and Electronic Structure Methods on Reaction Rates. Both the approach to transition state theory (IRC-TST, LC-TST, or MC-TST) and the level of electronic structure theory (B3LYP, ωB97X-D, F12-lowest, or F12-all) are important for the calculated reaction rate constants. The combined effect of varying these two parameters for the forward and reverse reactions is shown in Figure 7. The dashed horizontal line corresponds to the reference value obtained at the highest level: MC-TST at the F12-all level of electronic structure theory. For the IRC-TST results, the lowest-energy transition state is used, and for the MC-TST results, all unique conformers located in total are included.

A very clear trend is observed for this system: improving the level of electronic structure theory or the approach to transition state theory decreases the reaction rate constant for both reactions. The effect is most dramatic for the reverse reaction, with more than 8 orders of magnitude of difference between the highest and lowest values. For the forward reaction, the difference is 3 orders of magnitude. This means that in order to get accurate reaction rate constants, both transition state theory and electronic structure theory need to be applied at a high level. On the other hand, the results also suggest that if a reaction is too slow to matter at the B3LYP IRC-TST level, it can likely be disregarded completely, and this level is therefore useful for initial screening to eliminate slow reactions effectively. The overestimation of reaction rates by B3LYP relative to higher levels of electronic structure theory is in agreement with the literature.[12,82−84]

The difference between using F12 only for the reaction barrier, with ωB97X-D/aVTZ for the relative energies between conformers (F12-lowest), and using F12 single-point energies for all of the conformers (F12-all) is less than 20% for both the forward and reverse reactions. This suggests that for the relative energy between conformers, ωB97X-D/aVTZ is suitable, but in order to get an accurate barrier between the reactant and transition state, F12 is necessary. This means that only the lowest-energy conformers of the reactant, transition state, and product need F12 single-point calculations. The data on which the figure is based are found in Tables S10 and S11.

Effect of Cutoff on Reaction Rate. Despite the good results for MC-TST, computational limitations necessitate the use of approximations to the full MC-TST approach for most systems. The Boltzmann weight in the MC-TST expression means that only the low-energy conformers contribute significantly to the reaction rate, and considerable amounts of computational time are spent optimizing the high-energy conformers for the full MC-TST calculation. For MC-TST to be computationally viable, it is therefore important to reduce the number of conformers before the computationally demanding high-level calculations. To be able to do this while keeping the important low-energy conformers, a correlation between the relative energy of a given conformer at the different levels of theory is necessary; the stronger the correlation, the smaller is the risk of losing important conformers with a given cutoff. Similarly, the earlier the cutoff is introduced, the larger the computational savings.

In Figure 8, we show the correlation between the relative electronic energy (force field energy for MMFF) of the reactant conformers at the consecutive levels of theory: MMFF-charge,

DOI: 10.1021/acs.jpca.6b09370
J. Phys. Chem. A 2016, 120, 10072−10087

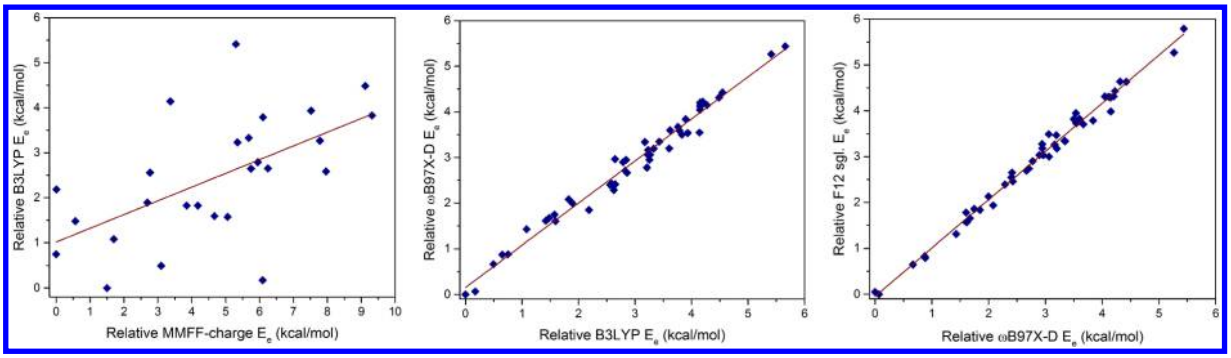

Figure 8. Correlation between relative energy of the unique reactant conformers at various levels of electronic structure theory calculated relative to the lowest-energy reactant at the given level. For the quantum-mechanical methods, the relative energies are based on the electronic energies of the optimized structures. In the left panel, only the conformers located with MMFF-charge are included, while the center and right panels include all of the conformers. The red line corresponds to a linear least-squares fit.

B3LYP, ωB97X-D and F12. While some correlation is observed between the molecular mechanics and optimized B3LYP energies, it is not very strong and shows several outliers. For large systems it may be necessary to introduce a cutoff directly following the molecular mechanics conformer search to avoid being overwhelmed, but it will be necessary to choose a reasonably high cutoff.

On the other hand, in Figure 8 we clearly see a very strong correlation between the relative energies of a given conformer for the remaining levels of electronic structure theory employed. The strength of the correlation between ωB97X-D/aVTZ and F12//ωB97X-D/aVTZ is likely partly due to the fact that they use the same (ωB97X-D/aVTZ) geometry, but this is how F12 will be employed in most calculations because of the very high computational cost of F12 optimizations. The strong correlation suggests that a cutoff after the B3LYP calculations will be a very reasonable way to save computational time with only a small risk of losing important low-energy conformers.

As shown in Figure 9, the correlation with the B3LYP-optimized energies is significantly better for B3LYP single-point energies than molecular mechanics energies (Figure 8, left panel). This shows that the molecular mechanics geometries are better than their energies, which is not surprising. For larger systems, for which a cutoff before B3LYP optimizations is necessary, using B3LYP single-point energies rather than molecular mechanics energies therefore seems to be a better choice in spite of the slightly higher computational cost.[17] Providing an actual value for such a cutoff is difficult because of the limited spread in energy of the conformers of this system, but from Figure 9, a 5 kcal/mol cutoff seems reasonable.

The strength of the correlation, however, for both molecular mechanics and B3LYP single-point energies depends very much on the choice of molecular mechanics method (see section S7.1). The trends for the product are similar to the ones presented here for the reactant (see section S7.1 and Table S20).

Figure 10 shows how a cutoff on electronic energies following B3LYP/6-31+G(d) optimizations affects the final MC-TST reaction rate constant calculated at the F12-all level. The rates in the figure were calculated by including all of the conformers below the cutoff, while all of the conformers above were excluded completely. The leftmost value corresponds to LC-TST, and the rightmost value corresponds to the full MC-TST approach. Also shown in the figure is the fraction of conformers excluded from further calculations as a function of the cutoff.

From Figure 10 it can be seen that even with a cutoff at a lower level of theory, relatively effective convergence is observed in the high-level MC-TST reaction rate. However, it is also clear that with a low energy cutoff, relatively large fluctuations in the calculated rate are observed. We tested the use of more computationally demanding levels to obtain the energy used for the cutoff, and while they significantly increased the computational cost, no clear improvement was observed for the calculated reaction rate constants (see Tables S21 and S22).

On the basis of the rapid convergence of the reaction rate constant with respect to an energy cutoff, we propose a cutoff of 2 kcal/mol at the B3LYP/6-31+G(d) optimized electronic energies, which is the earliest level of theory except for molecular mechanics and therefore provides the largest computational savings. For the forward reaction, this introduces an error of 10% in the calculated reaction rate constant while saving 70% of the ωB97X-D optimizations and frequency calculations, and for the reverse reaction, the deviation from full MC-TST is 14% while saving 72% of the ωB97X-D/aVTZ optimizations and frequency calculations. The deviations of the calculated reaction rate constants are small compared with the total expected uncertainty, especially considering the significant computational savings.

For larger systems with more transition states, the effect of cutting away reactant conformers will partly be canceled by cutting transition states, an effect we do not observe here because all four transition states are within the 2 kcal/mol cutoff. This would partly negate the deviation from full MC-TST caused by the cutoff.

As shown in Figure 7, only F12 calculation of the lowest-energy conformer of the reactant, transition state, and product is needed for accurate reaction rates. The high cost of doing even single-point calculations at the F12 level, especially for larger systems, means that ideally we would like to do only one F12 single-point calculation each for the reactant, product, and transition state. The very strong correlation between the relative energies at the ωB97X-D and F12 levels shown in Figure 8 suggests that doing only F12 single-point calculations of the lowest-energy conformers at the ωB97X-D level is unlikely to introduce large errors. For the product, however, the two lowest-energy conformers switch order after F12 single-point calculations. Using only an F12 single-point calculation of the single lowest-energy ωB97X-D conformer would underestimate the reverse reaction barrier by 0.34 kcal/mol, which

DOI: 10.1021/acs.jpca.6b09370
J. Phys. Chem. A 2016, 120, 10072−10087

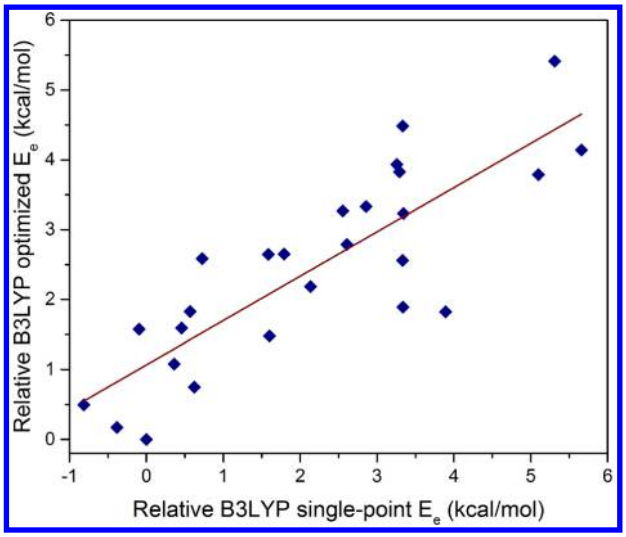

Figure 9. Correlation between B3LYP single-point electronic energies of all unique MMFF-charge reactant conformers and B3LYP electronic energies of the optimized conformers. The red line corresponds to a linear least-squares fit.

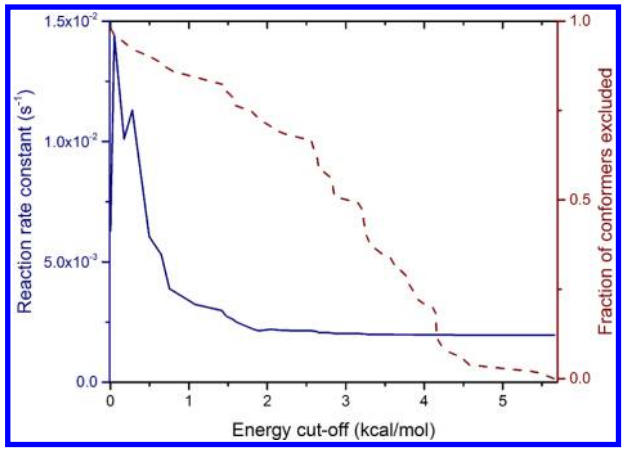

Figure 10. Forward reaction rate constant calculated using MC-TST with F12-all (blue, solid, left axis) and fraction of conformers excluded from later higher-level calculations (red, dashed, right axis) as a function of the energy cutoff placed at the B3LYP/6-31+G(d) electronic energy of optimized structures.

would increase the calculated reverse reaction rate constant by a factor of 1.77. The two conformers are within 0.05 kcal/mol of each other in terms of zero-point-corrected energy at the ωB97X-D/aVTZ level, so if possible, rather than doing the F12 single-point calculation of only the lowest-energy ωB97X-D conformer, a very tight energy cutoff at that level may be used to increase the chance of finding the lowest-energy conformer at the F12 level. However, generally we will assume that the error introduced by doing F12 single-point calculations of only the lowest-energy conformers at the ωB97X-D level is small, especially compared with the computational cost of doing more.

Effect of Conformer Weighting of Tunneling Coefficients. In Table 2, we show the F12/ωB97X-D Eckart tunneling coefficients obtained for the system's four transition states along with their relative zero-point-corrected F12 single-point energies and relative weights (ρ). The weight is defined as the Boltzmann factor multiplied by the partition function on the basis of the expression in the numerator of eq 3. The weighted average of the tunneling coefficients is also included in the table. For this system, all four Eckart tunneling coefficients are within a factor of 2.5 of each other, which suggests that a reasonably small error is introduced by using any of the tunneling coefficients. The similarity of the tunneling coefficients is not unexpected, as transition states for the same reaction tend to have similar imaginary frequencies. Furthermore, energy-lowering features of the transition state such as hydrogen bonds tend to remain in the IRC-connected reactant and product. This means that lower-energy conformers of the transition state often connect to lower-energy reactants and products, and similarly for higher-energy conformers, leading to similar barrier heights for the different IRCs (see Table S25).

Table 2 also shows that using the tunneling coefficient associated with the lowest-energy transition state is a good approach, as it represents nearly 50 percent of the total weight. The combination of the similarity of the tunneling coefficients and the large weight of the lowest-energy transition state in the calculation of the weighted tunneling coefficient means that using the coefficient of the lowest-energy transition state introduces an error of less than 25% relative to using the correctly weighted sum of all four tunneling coefficients. While the Eckart calculation itself is fast, it requires calculation of the IRC and F12-single point calculations of the end points, and thus, using a tunneling coefficient calculated from the lowest-energy transition state seems to be a reasonable approach considering the computational savings. For systems with a higher number of transition states and if more expensive tunneling approaches are employed, even larger computational savings will be obtained.

The Eckart tunneling coefficient obtained by using the lowest-energy conformers of the reactant, transition state, and product is 86.8 at the F12/ωB97X-D level of theory, which is close to the weighted tunneling coefficient of 79.3. Thus, for this system, using only the lowest-energy conformer of the reactant, transition state, and product to calculate the tunneling coefficient would also be a reasonable approach. Generally, however, this approach is expected to overestimate the tunneling, as the IRC from the lowest-energy transition state rarely connects to the lowest-energy conformers of the reactant and product.

As mentioned previously, assessment of different methods for calculating tunneling coefficients is beyond the scope of this work, but for the 1,4- and 1,5-hydrogen shifts in *n*-propylperoxy radicals it has been shown that Eckart tunneling is within a factor of 2.4 and 1.4, respectively, of the multidimensional small-curvature tunneling at 300 K.[66]

As shown in section S8.2, we found that IRCs obtained at the computationally much cheaper B3LYP/6-31+G(d) level have

Table 2. F12/ωB97X-D Eckart Tunneling Coefficients (κ) for the Four Transition States, Their Relative Zero-Point-Corrected Energies (in kcal/mol), and Their Relative Weights (ρ) Calculated as the Boltzmann Factor Multiplied by the Partition Function

	E_{rel}	ρ	κ
TS-1	0.00	0.49	60.4
TS-2	0.10	0.33	113.6
TS-3	0.76	0.15	56.5
TS-4	1.70	0.03	134.3
Weighted			79.3

DOI: 10.1021/acs.jpca.6b09370
J. Phys. Chem. A 2016, 120, 10072−10087

end points very similar to IRCs obtained at the ωB97X-D/aVTZ level. Therefore, we propose using IRCs at the B3LYP/6-31+G(d) level to locate the conformers to which the transition state is connected. These can then be optimized at the higher level and used for the Eckart tunneling calculation.

Summary of the Suggested Approach. The procedures for the various parts of the suggested approach can be summarized by the lists of steps shown below.

Initial sampling for the reactant and product:

1. MMFF systematic conformer search with the correct charge (0) enforced on the radical center (MMFF-charge). (The starting geometry can be a structure drawn by hand or a B3LYP/6-31+G(d)-optimized geometry).
2. (Option for larger systems: B3LYP/6-31+G(d) single-point calculation followed by 5 kcal/mol energy cutoff.)
3. B3LYP/6-31+G(d) optimization of all structures located in the conformer search.

Initial sampling for the transition state:

1. B3LYP/6-31+G(d) optimization of one transition state structure and frequency calculation to ensure that the structure corresponds to a TS for the reaction of interest.
2. MMFF systematic conformer search with the correct charge (0) enforced on the radical center (MMFF-charge) starting from the B3LYP/6-31+G(d)-optimized transition state structure and with the bond lengths of the bond being formed and broken as well as the OO bond constrained.
3. (Option for larger systems: B3LYP/6-31+G(d) single-point calculation followed by 5 kcal/mol energy cutoff.)
4. B3LYP/6-31+G(d) constrained optimization (toward a minimum) of all structures with the same constraints as in the conformer search.
5. Removal of duplicate conformers via energy and dipole moment (and, if possible, geometry deviation).
6. B3LYP/6-31+G(d) TS optimizations of all unique structures with frequency calculations to ensure that the structures correspond to the TS of interest.

Subsequent calculations for all structures:

1. Removal of duplicate conformers via energy and dipole moment (and, if possible, geometry deviation).
2. ωB97X-D/aVTZ optimization and frequency calculation of all unique conformers for which the B3LYP/6-31+G(d) electronic energy is within 2 kcal/mol of the lowest-energy conformer.
3. ROHF-ROCCSD(T)-F12a/cc-pVDZ-F12 (gem_beta = 0.9) single-point calculation of lowest-energy (zero-point-corrected) conformers of the reactant, transition state, and product at the ωB97X-D/aVTZ level of theory using the ωB97X-D/aVTZ geometries.
4. MC-TST reaction rate constant calculation using F12 single-point energies with ωB97X-D/aVTZ zero-point corrections for the reaction barrier and ωB97X-D/aVTZ for relative zero-point-corrected energies between conformers and partition functions (F12-lowest).

Further calculations for Eckart tunneling:

1. IRC at the B3LYP/6-31+G(d) level from the lowest-energy transition state at the ωB97X-D/aVTZ level, but starting from the B3LYP/6-31+G(d) geometry, and optimization of the end points using B3LYP/6-31+G(d).
2. ωB97X-D/aVTZ optimization of the B3LYP-optimized IRC end points, if it is a conformer not already optimized at that level.
3. F12 single-point calculation of the IRC end points using the ωB97X-D/aVTZ geometry.
4. Eckart tunneling coefficient calculation with the energy of the lowest-energy transition state and the corresponding optimized IRC end points calculated from F12 single-points with ωB97X-D/aVTZ zero-point vibrational energies and the imaginary frequency of the transition state calculated at the ωB97X-D/aVTZ level of theory.

The approach outlined above assumes that both the forward and reverse reactions are of interest. If only the forward reaction is studied, only the IRC end point is of interest for the product, as this is used in the calculation of the tunneling coefficient. Better tunneling approaches are available and may be employed instead of the Eckart approach outlined here. A flowchart of the suggested approach can be found in section S9.

Sensitivity and Assessment of the Approach. For the lowest-energy conformers of the reactant, transition state, and product, ROHF-ROCCSD(T)-F12a/cc-pVDZ-F12 optimizations were performed to assess the validity of using F12 single-point calculations rather than optimizations. These optimizations are orders of magnitude more computationally expensive than the single-point calculations, and only the small size of the test system allowed them to be carried out.

For the forward reaction, the F12-optimized reaction barrier is 0.24 kcal/mol higher than the barrier obtained using F12 single-point calculations, and for the reverse reaction, the difference is 0.33 kcal/mol in the same direction. For both the forward and reverse reactions, the rate obtained by using F12 single-point energies for the reaction barrier is within a factor of 2 (factors of 1.5 and 1.7, respectively) of the rate obtained using the F12-optimized energies. For both reactions, single-point calculations for the reaction barriers lead to overestimation of the reaction rate. The reasonably small difference highlights the quality of the ωB97X-D/aVTZ geometries, and as F12 optimizations are not feasible for larger systems, this error is likely inevitable. The results are summarized in Table S26.

The quality of the ωB97X-D/aVTZ geometries of the reactant, transition state, and product is further illustrated by the fact that the rotational partition functions are within 0.6% of those calculated using the F12-optimized geometries and the RMSD of the geometrical deviations is in each case below 0.04 Å (see Table S27).

For the ωB97X-D/aVTZ optimization, tests show that the "opt = verytight" keyword employed provides virtually no improvement in the rates constants compared with the cost (see section S10.4). We therefore suggest that this keyword should not be employed. The "int = ultrafine" keyword should still be used.

Uncoupled (Truhlar, Pitzer and Gwinn, and McClurg) and coupled (MS-T) hindered rotor calculations were performed to assess the error introduced by treating the anharmonic low-frequency torsions as harmonic oscillators. Relative to the MS-T value, which is the only coupled hindered rotor approach employed, the harmonic oscillator assumption seemingly overestimates the MC-TST F12-lowest forward and reverse reaction rates by 46 and 64%, respectively. Most of the effect, however, is caused by one transition state conformer having a seemingly unreasonably low coupled torsional barrier (see section S10.5). Eliminating this structure in both the harmonic

DOI: 10.1021/acs.jpca.6b09370
J. Phys. Chem. A 2016, 120, 10072−10087

oscillator and MS-T calculations reduces the overestimation by around two-thirds (to 12% and 24% for the forward and reverse reactions, respectively).

Similarly, the uncoupled (1D) hindered rotor approaches in Gaussian reduce the reaction rate relative to the harmonic oscillator approach. The Pitzer and Gwinn approach and the Truhlar method reduce the reaction rates by less than 15%, while the McClurg approach leads to reductions of around 30%. For three conformers, the Gaussian hindered rotor approach fails to achieve correspondence between the harmonic oscillator and hindered rotor vibrations. For these, the harmonic oscillator values have been used, but such observations are not particularly comforting. As the corrections are so relatively small and in view of the risk of seemingly unreasonable results and errors, we do not recommend the use of hindered rotor corrections, although that seems to lead to a small overestimation of the reaction rates. For a fuller discussion of the hindered rotor results, see section S10.5.

The reaction rate constants obtained with the approach outlined in this paper have been compared to the benchmark values obtained from MC-TST F12-all including all unique conformers, F12 optimizations for the energy barrier, tunneling from the four weighted Eckart tunneling coefficients, and the McClurg approach to hindered rotation (see Table S28). The latter was used because of the seemingly unreasonable result for MS-T and also because this is the most consistent of the methods implemented in Gaussian.[73] The benchmark reaction rate constants obtained using this approach are 7.99×10^{-2} and 5.85×10^{-1} s^{-1} for the forward and reverse reactions, respectively. The corresponding reaction rate constants obtained using our cost-effective approach are 1.68×10^{-1} and 1.26 s^{-1}. This corresponds to overestimations by factors of 2.1 and 2.2 for the forward and reverse reactions, respectively, relative to the benchmark.

For comparison, our approach saves 77% of the ωB97X-D/aVTZ optimization and frequency calculations and 96% of the F12 single-point calculations. Furthermore, it requires no F12 optimizations, which are orders of magnitude computationally more expensive than the other calculations and not feasible for systems much larger than the one studied here. The computational time saved in locating conformers and optimizing these with B3LYP is not easily quantified, as several different conformer searching methods are required to obtain all of the conformers, but it is similarly significant. For this system at atmospherically relevant temperatures, our approach therefore retains accuracy to within a factor of 2.5 relative to the benchmark calculation while reducing the computational cost by more than 90%, and similar performance is expected for other systems.

Assessment of the Approach at Elevated Temperatures. Hydrogen shift reactions are not only relevant under atmospheric conditions but have also been found to be important in low-temperature combustion chemistry.[21−24] We have assessed the performance of our suggested approach at a temperature of 1000 K.

The temperature dependence in the Boltzmann expression means that as the temperature increases, the higher-energy conformers become more populated and therefore more important. This naturally means that the errors introduced by a cutoff and incomplete conformer sampling of the high-energy conformers will both be larger. At 1000 K, the error from the cutoff increases by about 50 percentage points relative to that at 298.15 K, while the error from the incomplete conformer sampling increases by about 30 percentage points relative to that at 298.15 K (see Tables S36 and S37). At 298.15 K, a cutoff of 2 kcal/mol corresponds to 3.4RT, while at 1000 K the same cutoff corresponds to only 1RT, so at higher temperature a cutoff retaining the same value relative to RT is likely a better choice.

On the other hand, as a larger fraction of the molecules have sufficient energy to cross the barrier at 1000 K, tunneling becomes significantly smaller, and similarly, the error introduced by the tunneling coefficient decreases (Tables S38 and S39). At 1000 K, all of the tunneling coefficients are between 1.3 and 1.4. Using only the tunneling coefficient from the lowest-energy TS thus introduces an error of less than 2% relative to using the four weighted tunneling coefficients, compared with an error of 24% at 298.15 K. Even neglecting tunneling entirely causes an error of less than 40%.

The quality of the harmonic oscillator approximation decreases with increasing temperature, and therefore, the error introduced by neglecting hindered rotation is larger at 1000 K than at 298.15 K.[69] For the MC-TST F12-lowest reaction rate including all conformers, the overestimation of around 30% for the harmonic oscillator relative to the McClurg approach at 298.15 K increases to a factor of 2 at 1000 K for both the forward and reverse reactions (see Table S40).

In total, the approximations introduced in our approach act to overestimate the reaction rate more at 1000 K than at 298.15 K. At 1000 K, the forward and reverse rate constants are overestimated by factors of 5.3 and 7.0, respectively (see Table S41), which are significantly worse than the factors of 2.1 and 2.2 at 298.15 K.

At 500 K, the error introduced by the approach is between that at 298.15 and 1000 K (see section S12). At temperatures higher than 1000 K, the deviations introduced by the approximations in the outlined approach are expected to be even more pronounced. Therefore, while an approach similar to the one outlined here is possible at combustion temperatures, higher energy cutoffs and better treatment of internal torsions are needed in order to retain accuracy.

Application to Larger Systems. To further assess the approach outlined in this work, we have applied it to three peroxy radical hydrogen shift reactions for which experimental reaction rate constants are available in the literature. The first reaction (MACR) occurs in the autoxidation of methacrolein, and the second (3-PN-1) and third (3-PN-2) occur in the autoxidation of 3-pentanone.[6,11] The reaction of methacrolein is of direct atmospheric relevance, while the two pentanone reactions are used as models for atmospherically relevant reactions, and to show that autoxidation can be accelerated by substituents. The transition states of the three reactions are shown schematically in Table 3.

The three reactions span a range of molecular sizes (four and five carbon atoms and three to five oxygen atoms), functional groups (carbonyl, hydroxy, and hydroperoxy), and types of hydrogen shift (1,4-aldehydic and 1,5). As such, they represent a wide range of the peroxy radical hydrogen shifts important in atmospheric autoxidation.[6,11,16,17,18] Similar to the reaction studied in the test system, the MACR reaction is an aldehydic hydrogen shift, but the system size is increased by an additional carbon atom and the reaction is a 1,4-hydrogen shift as opposed to the 1,5-hydrogen shift of the test system. The pentanones have five carbon atoms and are non-aldehydic hydrogen shift reactions.

DOI: 10.1021/acs.jpca.6b09370
J. Phys. Chem. A 2016, 120, 10072−10087

Table 3. Reaction Rate Constants of Peroxy Radical Hydrogen Shift Reactions (in s^{-1}) Calculated Using the Approach Suggested in This Work Compared with Experimental Values from the Literature

Reaction	Hydrogen shift	MC-TST [a]	Experimental Value
MACR	1,4-aldehydic	0.48	0.5 [b]
3-PN-1	1,5	9.2×10^{-3}	$\leq 2\times10^{-3}$ [c]
3-PN-2 [d]	1,5	(*R*,*S*) 0.25 (*S*,*S*) 0.54	> 0.1 [c]

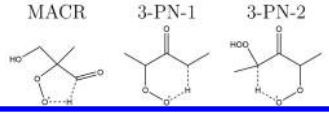

[a]This work using our suggested approach as described in Summary of the Suggested Approach. [b]Crounse et al.[11] [c]Crounse et al.[6] [d]The reactant of 3-PN-2 exists as two diastereomers. The reaction rate constant was calculated for both, while the experimental result was determined from a mixture of the two.

As can be seen in Table 3, the reaction rate constants obtained using the cost-effective approach outlined in this work are within a factor of 5 of the experimental values, which clearly highlights the usefulness and versatility of our approach for peroxy radical hydrogen shift reactions.

For these four calculated reaction rate constants, further calculations were carried out to assess some of the recommendations derived from the test system and the error introduced by the approximations in our suggested approach. Conformer sampling using a limited number of the molecular mechanics approaches that performed well for the test system confirmed that loss of conformers is almost inevitable when only one force field is used. However, MMFF-charge and SYBYL remain good choices for reactants, transition states, and products. All of the rates calculated with the conformers found by each of the different conformer searching methods are within a factor of 1.3 of the reaction rate obtained with all conformers located, and most are significantly better (see Figures S5−S7). The largest deviation is observed for the forward reaction of MACR with MMFF-charge and is due to one relatively low energy reactant conformer being missed, but the overall performance of MMFF-charge and SYBYL is comparable.

As observed for the test system, we find that IRC-TST at the B3LYP/6-31+G(d) level of theory represents an upper limit for the reaction rate constant that can be used to effectively eliminate slow reactions (see sections S13.3−4).

Finally, these additional reactions confirm that a 2 kcal/mol cutoff on electronic energy is suitable to save computational effort, as the error introduced is less than 20% for all of the reactions while more than half of the ωB97X-D/aVTZ calculations are saved (see section S13.5).

Extension of the approach to reactions different from peroxy radical hydrogen shifts has not been tested, but with small modifications it is expected to be valid for other unimolecular reactions at 298 K. These include alkoxy hydrogen shift reactions as well as for instance epoxide formation and unimolecular decomposition reactions such as OH, CO, or HO_2 loss. For systems similar to the organic radicals treated here, the accuracies of the quantum-chemical methods employed are expected to be comparable. Similarly, the cutoff value of 2 kcal/mol, which is primarily a consequence of the Boltzmann weight, is expected to be reasonable also for other types of reactions. The two key things to consider in applying this approach to other systems are the force field parameters to use and the constraints in the transition state conformer search. However, a good starting point for the latter is to constrain the lengths of the bonds that change the most among the reactant, transition state, and product.

Remaining Uncertainties. The results presented in this work for room-temperature calculations suggest that with the approach outlined, the error introduced by the conformer sampling and energy cutoff is likely within a factor of 2. However, if the lowest-energy conformer is missed, the error might be higher. Reduction in the uncertainty associated with the conformer sampling would probably require molecular mechanics methods parametrized to correctly treat radicals and transition state structures. This is expected to further save computational time for conformational sampling, especially for the transition state, by reducing the number of conformers reverting to the same structure after B3LYP optimization. At 298.15 K, the error introduced by the harmonic oscillator approach to internal torsion is also limited.

Relative to the F12-optimized values, the error in the energy barrier is expected to be smaller than 1 kcal/mol. We expect the ROHF-RCCSD(T)-F12a/cc-pVDZ-F12 value to be close to the actual barrier, but higher-level calculations such as CCSDT or larger basis sets for the F12 optimizations are not computationally possible even for our small test system.

The approximation of using only one tunneling coefficient seems to be reasonable. On the other hand, as we have not assessed calculation of the absolute tunneling coefficient, the accuracy of this cannot be fully evaluated. It has been shown that for similar hydrogen shift reactions, the Eckart tunneling coefficient is in reasonable agreement with the results of higher-level multidimensional tunneling approaches.[66] Nevertheless, our treatment of tunneling may represent the largest single remaining error source in the rate constant calculated using our approach at 298.15 K.

■ CONCLUSION

We have developed a cost-effective approach for calculating reaction rate constants of peroxy radical hydrogen shift reactions. For the conformational sampling of radical species, we find that all of the molecular mechanics and semiempirical methods tested have significant problems, which can, however, partly be overcome by manually changing the treatment of the radical atom in molecular mechanics sampling. Despite the limitation in locating conformers, most of the methods provide reaction rates in good agreement with the rate obtained with all conformers. We propose MMFF with the correct neutral charge enforced on the radical center for conformer searches of the radical species involved in peroxy radical hydrogen shift reactions. For the transition states, however, it is necessary to constrain certain bond lengths in the conformer search. For the calculation of accurate reaction rates, MC-TST with F12 single-point calculations for the barrier is needed, while ωB97X-D/aVTZ calculations are suitable for the relative energy between conformers. ωB97X-D is also used to calculate the partition functions and zero-point energy corrections to the electronic energy. Low-level calculations can be used to eliminate slow reactions, as improving the approach to transition state theory and the level of electronic structure theory are both found to decrease the calculated reaction rate significantly. To save computational time, an energy cutoff can be used to exclude

DOI: 10.1021/acs.jpca.6b09370
J. Phys. Chem. A 2016, 120, 10072−10087

high-energy conformers (at the B3LYP/6-31G+(d) level) from higher-level calculations. This only had a small effect on the reaction rate. Tunneling is important for hydrogen shift reactions, as it can increase reaction rates at 298 K significantly. The effect of tunneling can be approximated by using the tunneling coefficient associated with the lowest-energy transition state instead of calculating one for each of the transition states. Here we used the Eckart tunneling coefficient calculated from the lowest-energy transition state and the reactant and product connected to this via an IRC. Compared to our best available values, we find that our approach provides very good results (within a factor of 2.5) at very significantly reduced computational cost at 298.15 K. At elevated temperatures resembling combustion conditions, our approach deviates more from the benchmark value, and changes such as higher energy cutoffs and better treatment of torsional vibrations are likely required. At room temperature, our approach provides reaction rates within a factor of 5 of experimentally determined reaction rates for three peroxy radical hydrogen shift reactions, further highlighting its usefulness.

■ ASSOCIATED CONTENT

Supporting Information

The Supporting Information is available free of charge on the ACS Publications website at DOI: 10.1021/acs.jpca.6b09370.

Derivation of MC-TST; scripts for eliminating duplicate conformers; outline of the procedure for choosing cutoffs for identifying duplicate conformers; overview of conformers located with each conformer searching method; overview of conformers located by changing the charge and atom type for MMFF conformer searching; effect of the number of rotations in conformer searching; effect of the starting geometry for conformer searching; comparison of B3LYP and ωB97X-D for initial DFT optimization; effect of the number of constraints in TS conformer searching; differences in bond lengths of the reactant, transition state, and product; effect of constrained optimization before TS optimization; effect of the TS starting geometry in conformer searching; rate constants at different ab initio and TST levels; correlation between relative energies at various levels of theory; effect of the cutoff on the reaction rate constant and the number of conformers excluded; data for tunneling coefficients for the different transition states; effect of IRCs at various levels; flowchart of the suggested approach; energies and reaction rates with F12 single-point and F12-optimized energies; comparison of geometrical parameters of the ωB97X-D- and F12-optimized geometries; reaction rates with the suggested and best approaches; computational times and effect of the "opt = verytight" optimizations; rate constants with the various approaches to hindered rotation; results for assessment of the suggested approach at 500 and 1000 K; and results obtained for three additional peroxy hydrogen shift reactions with experimental reaction rate constants (PDF)

■ AUTHOR INFORMATION

Corresponding Author

*E-mail: hgk@chem.ku.dk. Phone:+45-35320334. Fax: +45-35320322.

ORCID

Noora Hyttinen: 0000-0002-6025-5959

Henrik G. Kjaergaard: 0000-0002-7275-8297

Notes

The authors declare no competing financial interest.

Gaussian log files of all unique ωB97X-D/aVTZ structures and scripts used for identifying duplicate conformers are available at http://www.erda.dk/public/archives/YXJjaGl2ZS02eDBrbF8=/published-archive.html.

■ ACKNOWLEDGMENTS

We acknowledge the helpfulness of Sean Ohlinger and the Spartan support staff, who were always willing to answer all of our questions remarkably quickly and precisely. We are grateful to Jimmy C. Kromann and Paul O. Wennberg for helpful discussions. We thank the Danish Center for Scientific Computing, the Center for Exploitation of Solar Energy, and the Academy of Finland for funding and the CSC IT Centre for Science for computer time.

■ REFERENCES

(1) Lamb, B.; Guenther, A.; Gay, D.; Westberg, H. A National Inventory of Biogenic Hydrocarbon Emissions. *Atmos. Environ. (1967-1989)* **1987**, *21*, 1695−1705.

(2) Guenther, A.; Hewitt, C. N.; Erickson, D.; Fall, R.; Geron, C.; Graedel, T.; Harley, P.; Klinger, L.; Lerdau, M.; Mckay, W. A.; et al. A Global Model of Natural Volatile Organic Compound Emissions. *J. Geophys. Res.* **1995**, *100*, 8873−8892.

(3) Piccot, S. D.; Watson, J. J.; Jones, J. W. A Global Inventory of Volatile Organic Compound Emissions from Anthropogenic Sources. *J. Geophys. Res. Atmos.* **1992**, *97*, 9897−9912.

(4) Kroll, J. H.; Seinfeld, J. H. Chemistry of Secondary Organic Aerosol: Formation and Evolution of Low-Volatility Organics in the Atmosphere. *Atmos. Environ.* **2008**, *42*, 3593−3624.

(5) IPCC. *Climate Change 2013: The Physical Science Basis. Contribution of Working Group I to the Fifth Assessment Report of the Intergovernmental Panel on Climate Change*; Cambridge University Press: Cambridge, U.K., 2013; p 1535.

(6) Crounse, J. D.; Nielsen, L. B.; Jørgensen, S.; Kjaergaard, H. G.; Wennberg, P. O. Autoxidation of Organic Compounds in the Atmosphere. *J. Phys. Chem. Lett.* **2013**, *4*, 3513−3520.

(7) Ehn, M.; Thornton, J.; Kleist, E.; Sipilä, M.; Junninen, H.; Pullinen, I.; Springer, M.; Rubach, F.; Tillmann, R.; Lee, B.; et al. A Large Source of Low-Volatility Secondary Organic Aerosol. *Nature* **2014**, *506*, 476−479.

(8) Eyring, H. The Activated Complex in Chemical Reactions. *J. Chem. Phys.* **1935**, *3*, 107−115.

(9) Evans, M. G.; Polanyi, M. Some Applications of the Transition State Method to the Calculation of Reaction Velocities, Especially in Solution. *Trans. Faraday Soc.* **1935**, *31*, 875−894.

(10) Fukui, K. The Path of Chemical Reactions - the IRC Approach. *Acc. Chem. Res.* **1981**, *14*, 363−368.

(11) Crounse, J. D.; Knap, H. C.; Ørnsø, K. B.; Jørgensen, S.; Paulot, F.; Kjaergaard, H. G.; Wennberg, P. O. Atmospheric Fate of Methacrolein. 1. Peroxy Radical Isomerization Following Addition of OH and O_2. *J. Phys. Chem. A* **2012**, *116*, 5756−5762.

(12) Knap, H. C.; Jørgensen, S.; Kjaergaard, H. G. Theoretical Investigation of the Hydrogen Shift Reactions in Peroxy Radicals Derived from the Atmospheric Decomposition of 3-methyl-3-buten-1-ol (MBO331). *Chem. Phys. Lett.* **2015**, *619*, 236−240.

(13) Vereecken, L.; Peeters, J. Theoretical Investigation of the Role of Intramolecular Hydrogen Bonding in β-Hydroxyethoxy and β-Hydroxyethylperoxy Radicals in the Tropospheric Oxidation of Ethene. *J. Phys. Chem. A* **1999**, *103*, 1768−1775.

DOI: 10.1021/acs.jpca.6b09370
J. Phys. Chem. A 2016, 120, 10072−10087

(14) Vereecken, L.; Peeters, J. The 1,5-H-Shift in 1-butoxy: A Case Study in the Rigorous Implementation of Transition State Theory for a Multirotamer System. *J. Chem. Phys.* **2003**, *119*, 5159−5170.
(15) Vereecken, L.; Peeters, J. A Theoretical Study of the OH-Initiated Gas-Phase Oxidation Mechanism of β-Pinene ($C_{10}H_{16}$): First Generation Products. *Phys. Chem. Chem. Phys.* **2012**, *14*, 3802−3815.
(16) Peeters, J.; Müller, J.-F.; Stavrakou, T.; Nguyen, V. S. Hydroxyl Radical Recycling in Isoprene Oxidation Driven by Hydrogen Bonding and Hydrogen Tunneling: The Upgraded LIM1Mechanism. *J. Phys. Chem. A* **2014**, *118*, 8625−8643.
(17) Rissanen, M. P.; Kurtén, T.; Sipilä, M.; Thornton, J. A.; Kangasluoma, J.; Sarnela, N.; Junninen, H.; Jørgensen, S.; Schallhart, S.; Kajos, M. K.; et al. The Formation of Highly Oxidized Multifunctional Products in the Ozonolysis of Cyclohexene. *J. Am. Chem. Soc.* **2014**, *136*, 15596−15606.
(18) Jørgensen, S.; Knap, H. C.; Otkjær, R. V.; Jensen, A. M.; Kjeldsen, M. L. H.; Wennberg, P. O.; Kjaergaard, H. G. Rapid Hydrogen Shift Scrambling in Hydroperoxy-Substituted Organic Peroxy Radicals. *J. Phys. Chem. A* **2016**, *120*, 266−275.
(19) Kurtén, T.; Rissanen, M. P.; Mackeprang, K.; Thornton, J. A.; Hyttinen, N.; Jørgensen, S.; Ehn, M.; Kjaergaard, H. G. Computational Study of Hydrogen Shifts and Ring-Opening Mechanisms in α-Pinene Ozonolysis Products. *J. Phys. Chem. A* **2015**, *119*, 11366−11375.
(20) Jensen, F. *Introduction to Computational Chemistry*, 2nd ed.; John Wiley & Sons: Chichester, U.K., 2007.
(21) Heiss, A.; Sahetchian, K. Isomerization Reactions of the n-C_4H_9O and n-OOC_4H_8OH Radicals in Oxygen. *Int. J. Chem. Kinet.* **1996**, *28*, 531−544.
(22) Curran, H. J.; Fischer, S. L.; Dryer, F. L. The Reaction Kinetics of Dimethyl Ether. II:Low-Temperature Oxidation in Flow Reactors. *Int. J. Chem. Kinet.* **2000**, *32*, 741−759.
(23) Fournet, R.; Battin-Leclerc, F.; Glaude, P. A.; Judenherc, B.; Warth, V.; Côme, G. M.; Scacchi, G.; Ristori, A.; Pengloan, G.; Dagaut, P.; et al. The Gas-Phase Oxidation of n-hexadecane. *Int. J. Chem. Kinet.* **2001**, *33*, 574−586.
(24) Sarathy, S. M.; Vranckx, S.; Yasunaga, K.; Mehl, M.; OSSwald, P.; Metcalfe, W. K.; Westbrook, C. K.; Pitz, W. J.; Kohse-Höinghaus, K.; Fernandes, R. X.; et al. A Comprehensive Chemical Kinetic Combustion Model for the Four Butanol Isomers. *Combust. Flame* **2012**, *159*, 2028−2055.
(25) Asatryan, R.; da Silva, G.; Bozzelli, J. W. Quantum Chemical Study of the Acrolein (CH_2CHCHO) + OH + O_2 Reactions. *J. Phys. Chem. A* **2010**, *114*, 8302−8311.
(26) *Spartan'14*; Wavefunction, Inc.: Irvine, CA, 2014.
(27) Halgren, T. A. Merck Molecular Force Field. I. Basis, Form, Scope, Parameterization, and Performance of MMFF94. *J. Comput. Chem.* **1996**, *17*, 490−519.
(28) Halgren, T. A. Merck Molecular Force Field. II. MMFF94 van der Waals and Electrostatic Parameters for Intermolecular Interactions. *J. Comput. Chem.* **1996**, *17*, 520−552.
(29) Halgren, T. A. Merck Molecular Force Field. III. Molecular Geometries and Vibrational Frequencies for MMFF94. *J. Comput. Chem.* **1996**, *17*, 553−586.
(30) Halgren, T. A.; Nachbar, R. B. Merck Molecular Force Field. IV. Conformational Energies and Geometries for MMFF94. *J. Comput. Chem.* **1996**, *17*, 587−615.
(31) Halgren, T. A. Merck Molecular Force Field. V. Extension of MMFF94 Using Experimental Data, Additional Computational Data, and Empirical Rules. *J. Comput. Chem.* **1996**, *17*, 616−641.
(32) Halgren, T. A. MMFF VII. Characterization of MMFF94, MMFF94s, and Other Widely Available Force Fields for Conformational Energies and for Intermolecular-Interaction Energies and Geometries. *J. Comput. Chem.* **1999**, *20*, 730−748.
(33) Clark, M.; Cramer, R. D.; Van Opdenbosch, N. Validation of the General Purpose Tripos 5.2 Force Field. *J. Comput. Chem.* **1989**, *10*, 982−1012.
(34) Dewar, M. J. S.; Zoebisch, E. G.; Healy, E. F.; Stewart, J. J. P. Development and Use of Quantum Mechanical Molecular Models. 76. AM1: a New General Purpose Quantum Mechanical Molecular Model. *J. Am. Chem. Soc.* **1985**, *107*, 3902−3909.
(35) Dewar, M. J. S.; Thiel, W. Ground States of Molecules. 38. The MNDO Method. Approximations and Parameters. *J. Am. Chem. Soc.* **1977**, *99*, 4899−4907.
(36) Stewart, J. J. P. Optimization of Parameters for Semiempirical Methods II. Applications. *J. Comput. Chem.* **1989**, *10*, 221−264.
(37) Stewart, J. J. Optimization of Parameters for Semiempirical Methods V: Modification of NDDO Approximations and Application to 70 Elements. *J. Mol. Model.* **2007**, *13*, 1173−1213.
(38) Rocha, G. B.; Freire, R. O.; Simas, A. M.; Stewart, J. J. P. RM1: A Reparameterization of AM1 for H, C, N, O, P, S, F, Cl, Br, and I. *J. Comput. Chem.* **2006**, *27*, 1101−1111.
(39) Becke, A. D. Density-Functional Thermochemistry. III The Role of Exact Exchange. *J. Chem. Phys.* **1993**, *98*, 5648−5652.
(40) Lee, C.; Yang, W.; Parr, R. G. Development of the Colle-Salvetti Correlation-Energy Formula into a Functional of the Electron Density. *Phys. Rev. B: Condens. Matter Mater. Phys.* **1988**, *37*, 785−789.
(41) Yanai, T.; Tew, D. P.; Handy, N. C. A New Hybrid Exchange-Correlation Functional Using the Coulomb-Attenuating Method (CAM-B3LYP). *Chem. Phys. Lett.* **2004**, *393*, 51−57.
(42) Zhao, Y.; Truhlar, D. G. Density Functionals with Broad Applicability in Chemistry. *Acc. Chem. Res.* **2008**, *41*, 157−167.
(43) Holroyd, L. F.; van Mourik, T. Insufficient Description of Dispersion in B3LYP and Large Basis Set Superposition Errors in MP2 Calculations Can Hide Peptide Conformers. *Chem. Phys. Lett.* **2007**, *442*, 42−46.
(44) Garden, A. L.; Paulot, F.; Crounse, J. D.; Maxwell-Cameron, I. J.; Wennberg, P. O.; Kjaergaard, H. G. Calculation of Conformationally Weighted Dipole Moments Useful in Ion−Molecule Collision Rate Estimates. *Chem. Phys. Lett.* **2009**, *474*, 45−50.
(45) Hyttinen, N.; Kupiainen-Määttä, O.; Rissanen, M. P.; Muuronen, M.; Ehn, M.; Kurtén, T. Modeling the Charging of Highly Oxidized Cyclohexene Ozonolysis Products Using Nitrate-Based Chemical Ionization. *J. Phys. Chem. A* **2015**, *119*, 6339−6345.
(46) Eksterowicz, J. E.; Houk, K. N. Transition-State Modeling with Empirical Force Fields. *Chem. Rev.* **1993**, *93*, 2439−2461.
(47) Hansen, E.; Rosales, A. R.; Tutkowski, B.; Norrby, P.-O.; Wiest, O. Prediction of Stereochemistry Using Q2MM. *Acc. Chem. Res.* **2016**, *49*, 996−1005.
(48) Mayo, S. L.; Olafson, B. D.; Goddard, W. A. DREIDING: A Generic Force Field for Molecular Simulations. *J. Phys. Chem.* **1990**, *94*, 8897−8909.
(49) Rappe, A. K.; Casewit, C. J.; Colwell, K. S.; Goddard, W. A.; Skiff, W. M. UFF, a Full Periodic Table Force Field for Molecular Mechanics and Molecular Dynamics Simulations. *J. Am. Chem. Soc.* **1992**, *114*, 10024−10035.
(50) Cornell, W. D.; Cieplak, P.; Bayly, C. I.; Gould, I. R.; Merz, K. M.; Ferguson, D. M.; Spellmeyer, D. C.; Fox, T.; Caldwell, J. W.; Kollman, P. A. A Second Generation Force Field for the Simulation of Proteins, Nucleic Acids, and Organic Molecules. *J. Am. Chem. Soc.* **1995**, *117*, 5179−5197.
(51) Frisch, M. J.; Trucks, G. W.; Schlegel, H. B.; Scuseria, G. E.; Robb, M. A.; Cheeseman, J. R.; Scalmani, G.; Barone, V.; Mennucci, B.; Petersson, G. A.; et al. *Gaussian 09*, revision D.01; Gaussian, Inc.: Wallingford, CT, 2009.
(52) Chai, J.-D.; Head-Gordon, M. Long-Range Corrected Hybrid Density Functionals with Damped Atom-Atom Dispersion Corrections. *Phys. Chem. Chem. Phys.* **2008**, *10*, 6615−6620.
(53) Hehre, W. J.; Ditchfield, R.; Pople, J. A. Self—Consistent Molecular Orbital Methods. XII. Further Extensions of Gaussian—Type Basis Sets for Use in Molecular Orbital Studies of Organic Molecules. *J. Chem. Phys.* **1972**, *56*, 2257−2261.
(54) Clark, T.; Chandrasekhar, J.; Spitznagel, G. W.; Schleyer, P. V. R. Efficient Diffuse Function-Augmented Basis Sets for Anion Calculations. III. The 3-21+G Basis Set for First-Row Elements, Li-F. *J. Comput. Chem.* **1983**, *4*, 294−301.

DOI: 10.1021/acs.jpca.6b09370
J. Phys. Chem. A 2016, 120, 10072−10087

(55) Frisch, M. J.; Pople, J. A.; Binkley, J. S. Self-Consistent Molecular Orbital Methods 25. Supplementary Functions for Gaussian Basis Sets. *J. Chem. Phys.* **1984**, *80*, 3265−3269.
(56) Dunning, T. H. Gaussian Basis Sets for Use in Correlated Molecular Calculations. I. The Atoms Boron Through Neon and Hydrogen. *J. Chem. Phys.* **1989**, *90*, 1007−1023.
(57) Kendall, R. A.; Dunning, T. H.; Harrison, R. J. Electron Affinities of the First-Row Atoms Revisited. Systematic Basis Sets and Wave Functions. *J. Chem. Phys.* **1992**, *96*, 6796−6806.
(58) Werner, H.-J.; Knowles, P. J.; Knizia, G.; Manby, F. R.; Schütz, M.; Celani, P.; Györffy, W.; Kats, D.; Korona, T.; Lindh, R.; et al. *MOLPRO: A Package of Ab Initio Programs*, version 1, 2012; http://www.molpro.net.
(59) Watts, J. D.; Gauss, J.; Bartlett, R. J. Coupled-Cluster Methods with Noniterative Triple Excitations for Restricted Open-Shell Hartree-Fock and Other General Single Determinant Reference Functions. Energies and Analytical Gradients. *J. Chem. Phys.* **1993**, *98*, 8718−8733.
(60) Adler, T. B.; Knizia, G.; Werner, H.-J. A Simple and Efficient CCSD(T)-F12 Approximation. *J. Chem. Phys.* **2007**, *127*, 221106.
(61) Knizia, G.; Adler, T. B.; Werner, H.-J. Simplified CCSD(T)-F12 Methods: Theory and Benchmarks. *J. Chem. Phys.* **2009**, *130*, 054104.
(62) Werner, H.-J.; Knizia, G.; Manby, F. R. Explicitly Correlated Coupled Cluster Methods with Pair-Specific Geminals. *Mol. Phys.* **2011**, *109*, 407−417.
(63) Peterson, K. A.; Adler, T. B.; Werner, H.-J. Systematically Convergent Basis Sets for Explicitly Correlated Wavefunctions: The Atoms H, He, B−Ne, and Al−Ar. *J. Chem. Phys.* **2008**, *128*, 084102.
(64) McMahon, R. J. Chemical Reactions Involving Quantum Tunneling. *Science* **2003**, *299*, 833−834.
(65) Eckart, C. The Penetration of a Potential Barrier by Electrons. *Phys. Rev.* **1930**, *35*, 1303−1309.
(66) Zhang, F.; Dibble, T. S. Impact of Tunneling on Hydrogen-Migration of the *n*-Propylperoxy Radical. *Phys. Chem. Chem. Phys.* **2011**, *13*, 17969−17977.
(67) Skodje, R. T.; Truhlar, D. G.; Garrett, B. C. A General Small-Curvature Approximation for Transition-State-Theory Transmission Coefficients. *J. Phys. Chem.* **1981**, *85*, 3019−3023.
(68) *MATLAB*, version 8.1.0.604 (R2013a); The MathWorks, Inc.: Natick, MA, 2013.
(69) Ayala, P. Y.; Schlegel, H. B. Identification and Treatment of Internal Rotation in Normal Mode Vibrational Analysis. *J. Chem. Phys.* **1998**, *108*, 2314−2325.
(70) Pitzer, K. S.; Gwinn, W. D. Energy Levels and Thermodynamic Functions for Molecules with Internal Rotation I. Rigid Frame with Attached Tops. *J. Chem. Phys.* **1942**, *10*, 428−440.
(71) Truhlar, D. G. A. Simple Approximation for the Vibrational Partition Function of a Hindered Internal Rotation. *J. Comput. Chem.* **1991**, *12*, 266−270.
(72) McClurg, R. B.; Flagan, R. C.; Goddard, W. A., III .The Hindered Rotor Density-of-States Interpolation Function. *J. Chem. Phys.* **1997**, *106*, 6675−6680.
(73) McClurg, R. B. Comment on: "The Hindered Rotor Density-of-States Interpolation Function" [J. Chem. Phys. 106, 6675 (1997)] and "The Hindered Rotor Density-of-States" [J. Chem. Phys. 108, 2314 (1998)]. *J. Chem. Phys.* **1999**, *111*, 7163−7164.
(74) Zheng, J.; Yu, T.; Papajak, E.; Alecu, I. M.; Mielke, S. L.; Truhlar, D. G. Practical Methods for Including Torsional Anharmonicity in Thermochemical Calculations on Complex Molecules: The Internal-Coordinate Multi-Structural Approximation. *Phys. Chem. Chem. Phys.* **2011**, *13*, 10885−10907.
(75) Zheng, J.; Mielke, S. L.; Clarkson, K. L.; Truhlar, D. G. MSTor: A Program for Calculating Partition Functions, Free Energies, Enthalpies, Entropies, and Heat Capacities of Complex Molecules Including Torsional Anharmonicity. *Comput. Phys. Commun.* **2012**, *183*, 1803−1812.
(76) Zheng, J.; Truhlar, D. G. Quantum Thermochemistry: Multistructural Method with Torsional Anharmonicity Based on a Coupled Torsional Potential. *J. Chem. Theory Comput.* **2013**, *9*, 1356−1367.
(77) Zheng, J.; Meana-Pañeda, R.; Truhlar, D. G. MSTor Version 2013: A new Version of the Computer Code for the Multi-Structural Torsional Anharmonicity, now with a Coupled Torsional Potential. *Comput. Phys. Commun.* **2013**, *184*, 2032−2033.
(78) Ellingson, B. A.; Lynch, V. A.; Mielke, S. L.; Truhlar, D. G. Statistical Thermodynamics of Bond Torsional Modes: Tests of Separable, Almost-Separable, and Improved Pitzer-Gwinn Approximations. *J. Chem. Phys.* **2006**, *125*, 084305.
(79) Lin, C. Y.; Izgorodina, E. I.; Coote, M. L. How Accurate Are Approximate Methods for Evaluating Partition Functions for Hindered Internal Rotations? *J. Phys. Chem. A* **2008**, *112*, 1956−1964.
(80) Kabsch, W. A Solution for the Best Rotation to Relate Two Sets of Vectors. *Acta Crystallogr., Sect. A: Cryst. Phys., Diffr., Theor. Gen. Crystallogr.* **1976**, *32*, 922−923.
(81) Kromann, J. C. GitHub: Calculate RMSD for Two XYZ Structures. http://github.com/charnley/rmsd.
(82) Lynch, B. J.; Truhlar, D. G. How Well Can Hybrid Density Functional Methods Predict Transition State Geometries and Barrier Heights? *J. Phys. Chem. A* **2001**, *105*, 2936−2941.
(83) Zhao, Y.; González-García, N.; Truhlar, D. G. Benchmark Database of Barrier Heights for Heavy Atom Transfer, Nucleophilic Substitution, Association, and Unimolecular Reactions and Its Use to Test Theoretical Methods. *J. Phys. Chem. A* **2005**, *109*, 2012−2018.
(84) Black, G.; Simmie, J. M. Barrier Heights for H-Atom Abstraction by $H\dot{O}_2$ from *n*-butanol−A Simple yet Exacting Test for Model Chemistries? *J. Comput. Chem.* **2010**, *31*, 1236−1248.

DOI: 10.1021/acs.jpca.6b09370
J. Phys. Chem. A 2016, 120, 10072−10087